NANO LETTERS

2007
Vol. 7, No. 8
2258−2262

Nanometer-Scale Dielectric Imaging of Semiconductor Nanoparticles: Size-Dependent Dipolar Coupling and Contrast Reversal

Zee Hwan Kim and Sung-Hyun Ahn

Department of Chemistry and Center for Electro- and Photo-Responsive Molecules, Korea University, Anam-Dong, Seongbuk-Gu, Seoul 136-701, Republic of Korea

Bing Liu[†] and Stephen R. Leone*

Department of Chemistry and Physics, University of California, and Lawrence Berkeley National Laboratory, Berkeley, California 94720-1460

Received March 30, 2007; Revised Manuscript Received June 10, 2007

ABSTRACT

Scattering-type apertureless near-field microscopy (ANSOM) provides high-resolution dielectric maps of indium gallium nitride (InGaN) semiconductor nanoparticles at visible (633 nm) wavelengths. A specific size-dependent contrast reversal is observed in the ANSOM images of InGaN nanoparticles grown on a layer of gallium nitride (GaN). Model calculations demonstrate that the observed contrast reversal is the result of the competition between the tip–particle versus tip–substrate dipolar coupling.

Apertureless near-field scanning optical microscopy (ANSOM), which relies on the localized field enhancement at the apex of tips, provides sub-20 nm spatial resolution images of nanostructures and single molecules via Raman, fluorescence, and scattering detection methods.[1−20]

Especially, the scattering-type ANSOM (hereafter called ANSOM for short) relies on the material-dependent tip−sample coupling as the chemically specific contrast mechanism. Thus far, ANSOM image contrasts of isolated metallic,[2,21,22] semiconducting,[6,11,23] and polymeric[1,8,12,14−17] nanostructures have been successfully explained via a simple dipole−image dipole coupling model in which the tip acts as a point dipole interacting with its own image formed on flat nano-object surfaces. However, in some classes of nano-objects on sample surfaces, the near-field coupling between the tip and the nano-objects, and hence the ANSOM image, are likely to be affected by the local environment (such as the substrate and nearby nanostructures) in which the nanostructure is located. However, very few experimental reports explore this nontrivial coupling in the ANSOM image formation. Cvitkovic et al.[2] recently demonstrated infrared imaging of single nanoparticles placed between the strongly interacting SiC substrate and metallic tip, demonstrating the importance of the substrate in ANSOM imaging.

In this work, we report a specific size-dependent contrast reversal observed in ANSOM images of InGaN semiconductor particles on a GaN layer. We explain the observed contrast reversal in terms of the competing roles of tip−substrate versus tip−particle couplings. The interpretation is further supported by a self-consistent Green's dyadic propagator[24] simulation of the ANSOM images.

The details of the ANSOM instrument (Figure 1) and its operating principles are already described elsewhere.[7] The Pt−Ti coated atomic force microscopy (AFM) tip is dithered near the resonance frequency of the cantilever ($\Omega \sim$ 300 kHz) with full amplitude of 20−100 nm above the sample surface. Linearly polarized (p-polarized with respect to the sample surface) light from a laser (HeNe, 632.8 nm) is focused onto the tip−sample junction with an angle of 30° with respect to the sample surface via an objective lens. Back-scattered light from the junction is collected by the same lens and homodyne-detected to give separate intensity and phase information of the scattered field. The far-field background signal that originates from scattering by the sample surface and tip shaft is removed by the third harmonic ($3\Omega \sim$ 900 kHz) demodulation technique via a lock-in amplifier. The optical and AFM topography images are simultaneously acquired by raster-scanning the sample and

* Corresponding author. Stephen R. Leone, srl@uclink.berkeley.edu. Telephone: (510)-643-5467. Fax 510-642-1376.
[†] Present address: IMRA America Inc., 1044 Woodridge Avenue, Ann Arbor, Michigan 48105.

10.1021/nl070753k CCC: $37.00
Published on Web 07/03/2007

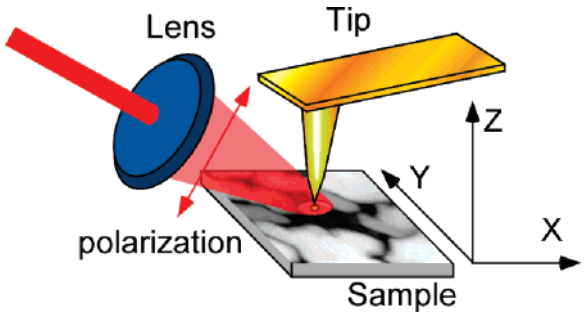

Figure 1. Schematic diagram of ANSOM instrument and coordinate system used throughout this work.

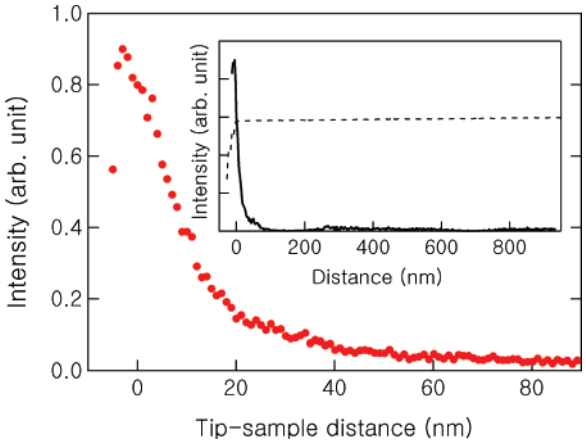

Figure 2. ANSOM intensity (I_3) approach curve (red circles), collected at the third harmonic of the tip oscillation frequency, above a InGaN particle (red circles). Inset: third harmonic signal approach curve (black solid) obtained on a larger tip−sample distance scale. Also shown in the inset with the dashed line is the cantilever tapping amplitude.

recording the optical and topographic signals. The samples of indium gallium nitride (InGaN) particles on a layer of gallium nitride (GaN) are grown by plasma-assisted molecular beam epitaxy (MBE) on sapphire (0001) substrates. The ensemble-averaged indium content of the $In_xGa_{1-x}N$ is around 20% ($x = 0.2$), as determined by X-ray diffraction. Different growth temperatures lead to InGaN nanoparticles with different average sizes (∼20 and ∼150 nm).

Figure 2 displays a third harmonic demodulation ANSOM approach curve (scattered optical signal intensity, $I_3 = |E_3|^2$, as a function of tip−particle distance) above an InGaN particle. The short decay length (∼10 nm) of the ANSOM signal with tip height above the particle corresponds to the distance scale at which the illuminated sample and the tip produce mutual perturbation of the respective near-field (tip−sample coupling), which therefore corresponds to the lateral spatial resolution of the ANSOM images. Approach curves taken at a longer distance scale (Figure 2 inset) ensure that the demodulated third harmonic signal does not have any oscillatory far-field background.[7] The low-dielectric materials (such as glasses or polymers) couple weakly with a metallic tip and often lead to topography-related artifacts.[26,27] In our case, however, InGaN and GaN have relatively large dielectric constants and couple strongly with a metallic tip. Combined use of third harmonic demodulation and homodyne interferometry allows us to suppress[25] the topography artifacts in the images.

Figure 3 shows AFM topographic and ANSOM images (third harmonic intensity and phase) of large (100−200 nm) and small (10−20 nm) InGaN particles on flat GaN layers. The ANSOM phase measures the optical phase difference between the input and back-scattered light and provides extra information on the near-field tip−sample coupling.[25] In AFM images, the InGaN particles appear as spheres of ∼100 or ∼10 nm in diameter. The tip-convolution effect causes appreciable lateral broadening in AFM images of the small particles. Therefore, the height information, not the lateral-size of the AFM image, is used to judge the size of the particles. Also, the InGaN particles can assume nonspherical shapes, which can be visible on a higher resolution scale. However, we find that fine structures of the particles can be neglected in interpreting ANSOM images. The GaN buffer layer is typically covered with a wetting layer of indium with a few monolayers of thickness. We can safely assume[28] that the scattering signal from the GaN layer (with a thickness larger than 200 nm) is dominantly determined by the bulk GaN and not by the thin wetting layer (less than a few nanometers) of indium that may be present above the GaN substrate. The InGaN has a slightly larger bulk dielectric constant than that of the GaN ($\epsilon_{InGaN} = 5.28 + 0.17i$ versus $\epsilon_{GaN} = 4.67 + 0.4 \times 10^{-4}i$).[29,30] Therefore, we expect the tip to couple more strongly with the InGaN particle than with the GaN substrate and hence will produce positive ANSOM intensity contrast (more signal) for InGaN against the GaN substrate. Indeed, large InGaN particles show strong positive contrast (signal ratio InGaN:GaN ∼ 3:1) against the GaN substrate (Figure 3b). Surprisingly, however, small InGaN particles show *negative* contrast (Figure 3e) against the GaN layer (signal ratio InGaN:GaN ∼ 1:3).

The ANSOM phase images for large and small InGaN particles also show qualitatively different features (Figure 3c,f). Specifically, the image of the large particles shows a nearly linear phase gradient along the illumination direction. On the other hand, the image of small particles does not show any directionality of the phase with respect to the illumination direction. Figure 4 shows the line profiles for the ANSOM phase and signal intensity along the lines (x-axis) indicated in Figure 3c,f. The ANSOM phase line profile for large InGaN particles shows a clearly visible linear gradient of ∼1°/ nm across each particle, whereas the corresponding line profile for small InGaN particles shows rather flat bumps across the centers of particles.

In general, the ANSOM scattering phase variation originates from the phase shift of sample dipole oscillation (either an image dipole on a flat substrate or a real dipole on the particle) with respect to the tip dipole phase. The tip image dipole is always located just below the tip and the phase of the image dipole oscillation is completely determined by the local dielectric constant of the sample and the tip−sample separation. Therefore, the ANSOM phase formed through the image dipole formation is *independent* of the illumination direction. On the other hand, a particle on the surface experiences different excitation phases depending on the

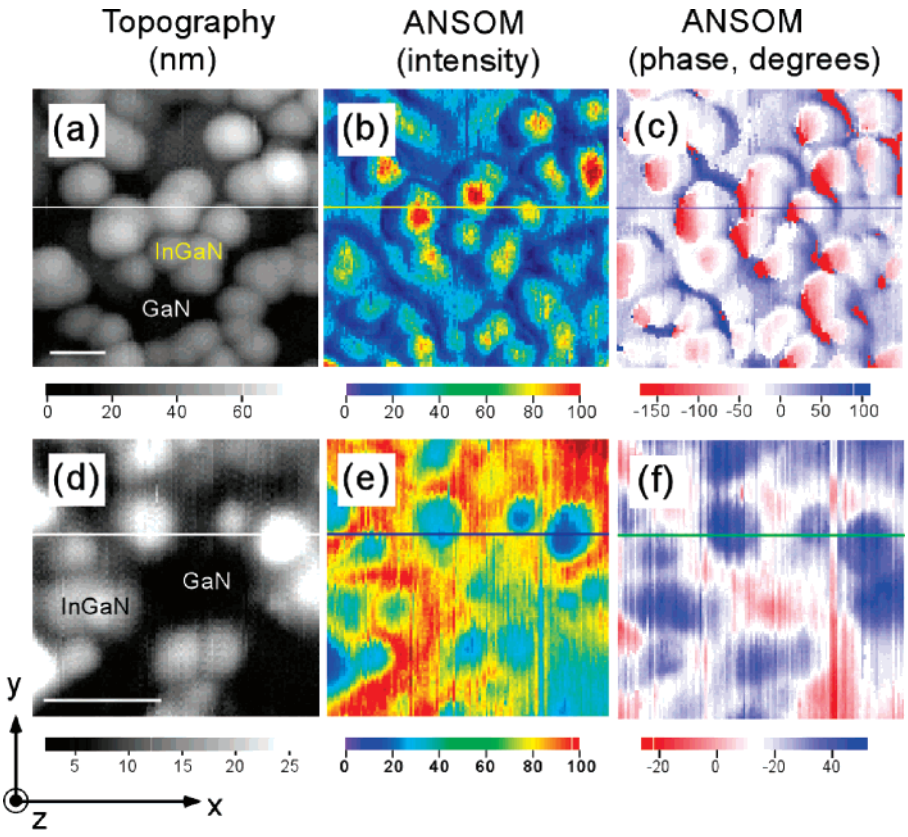

Figure 3. Selected regions of the AFM, ANSOM (third harmonic intensity) intensity, and ANSOM (third harmonic phase) intensity images of the large (a, b, and c) and small (d, e, and f) InGaN particles on InGaN surfaces. Scale bars on (a) and (d) both correspond to 100 nm. Horizontal lines in images indicate the positions of the line profiles shown in Figure 4. Also shown is the coordinate with respect to the illumination direction.

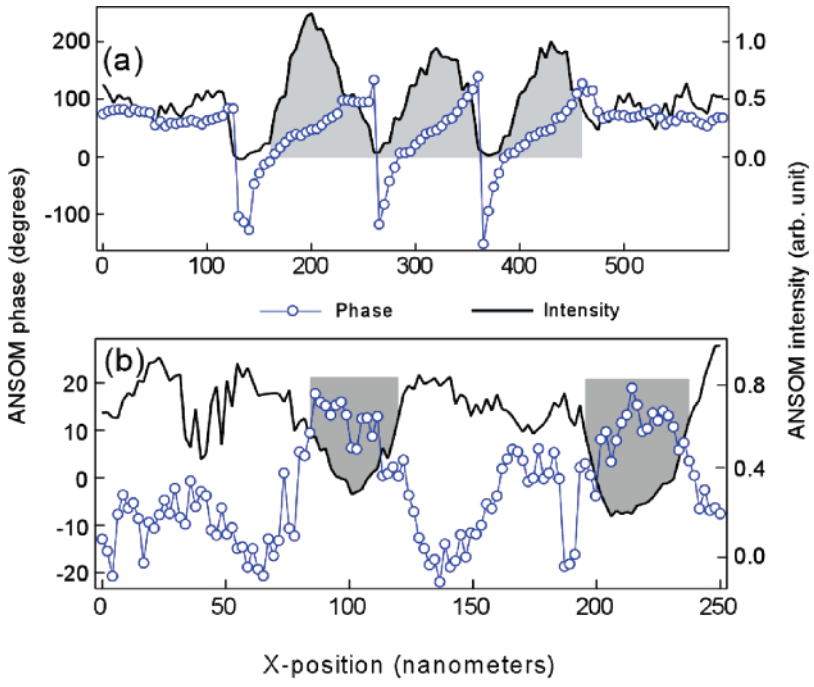

Figure 4. Line profiles of the ANSOM intensity (black lines) and ANSOM phase (blue open circles) images of large (a) and small (b) InGaN particles samples indicated in Figure 3. Shaded regions in the ANSOM intensity graph indicate the positions of the InGaN particles.

relative displacement from the tip and the wavefront of the illuminating light ($\delta = \vec{k}\cdot(\vec{r}_{\text{particle}} - \vec{r}_{\text{tip}})$, where $\vec{k}$ is the wave vector of the excitation beam, and $\vec{r}_{\text{particle}}$ and $\vec{r}_{\text{tip}}$ are the displacement vectors for the particle and the tip, respectively).[21] Therefore, the ANSOM phase formed through the direct tip−particle coupling is *dependent* on the illumination

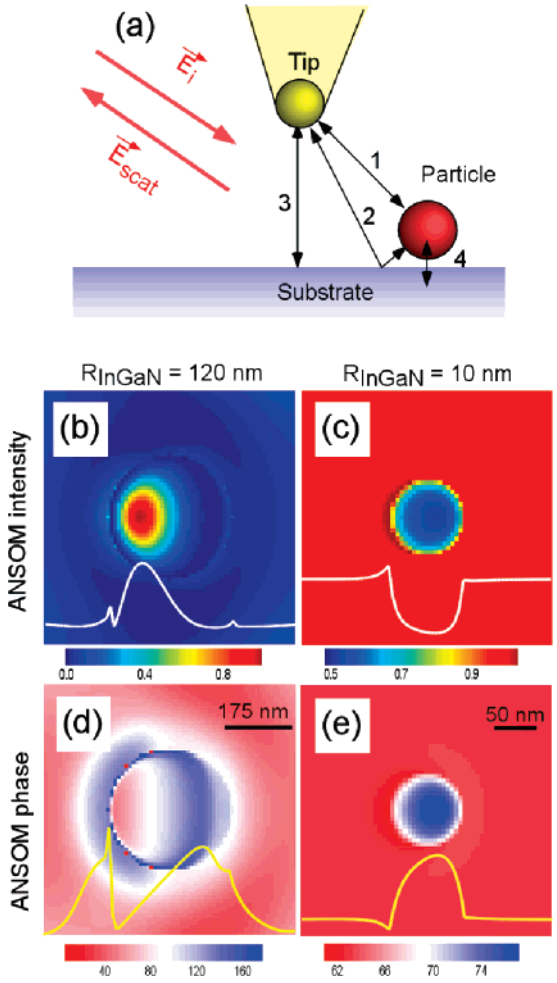

Figure 5. (a) Tip−sample coupling included in our simulation: (1) direct tip−particle interaction, (2) indirect tip−particle interaction, (3) tip−tip image interaction, and (4) particle−particle image interaction. Incident plane wave excites the system at an angle of 30° from the surface, and the scattered field is calculated. (b−e) Simulated ANSOM intensity and phase images of large (120 nm radius, b and d) and small (10 nm radius, c and e) InGaN particles. Also shown in white and yellow lines are the line profiles along the illumination direction (*x*-axis). The radius of the tip (Pt−Ti) is 50 nm.

direction. On the basis of the above arguments, we believe that the ANSOM image for the large particles is most likely formed via the direct tip dipole−particle dipole coupling, whereas the ANSOM image for small particles is formed via a tip dipole−image dipole mechanism.

To understand how the competition of these two mechanisms leads to the contrast reversal, we carried out a numerical simulation of the ANSOM images using the self-consistent Green's dyadic propagator method.[24] In this simulation, the tip dipole and the sample (particle + substrate) interact with each other via (1) direct tip−particle coupling, (2) tip−particle coupling through image dipoles, (3) tip−tip image coupling, and (4) The particle−particle image coupling (see Figure 5a). Parts b−e of Figure 5 display simulated ANSOM images and phases of large (Figure 5b,d) and small (Figure 5c,e) InGaN particles, together with the corresponding line profiles of the intensity and phase along

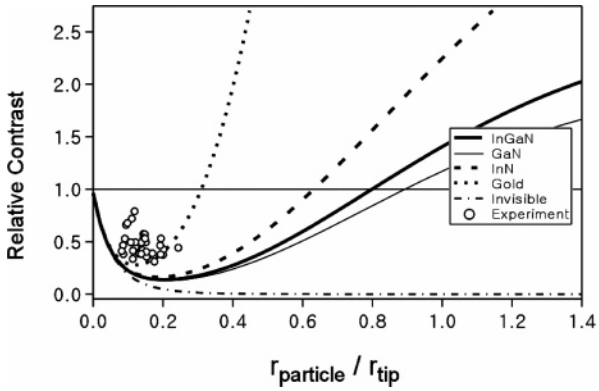

Figure 6. Simulated relative contrasts (ANSOM intensity of particle/ANSOM intensity of GaN substrate) of particles with different dielectric constants plotted as a function of particle:tip radius ratio (Thick solid line = InGaN, thin solid line = GaN, dashed line = InN, dotted line = Au, and dash−dot line = unit dielectric constant). Also shown in open circles is the experimental InGaN particle contrast vs radii of particles.

the illumination direction. The simulated images correctly capture the essential features of the experimental ANSOM images: (1) The InGaN particle with a large radius shows positive contrast, whereas a small one shows negative contrast. (2) Large particles show a phase gradient along the illumination direction, but the small ones do not have any directionality. The simulation neglects the contribution of higher multipole moments and the effects of electric field propagation *through* the finite volume of the tip and the particles. Nevertheless, the simulated images faithfully reproduce the experimentally observed contrast reversal and the phase gradient and support the proposed mechanism of the tip, particle, and substrate coupling in the ANSOM images (see below).

Figure 6 displays simulated intensity contrast ratios of GaN, InGaN, InN, and gold nanoparticles versus a GaN substrate plotted as a function of the radii of the particles. Also plotted is the corresponding curve for hypothetical nanoparticle with a unit dielectric constant (invisible particle). The simulation indicates that InGaN particles with radii larger than 80% of the tip radius will show positive contrast (relative contrast > 1), whereas the ones smaller than this critical size will show negative contrast. Also shown in Figure 6 is the experimental correlation between the radii of the particles versus their ANSOM contrasts (35 randomly selected InGaN particles), which show a reasonable agreement with our model calculation.

Interestingly, this size-dependent contrast change is rather insensitive to the change in dielectric constants and hence chemical compositions of the nanoparticles. For example (see Figure 6), the InN (100% indium content), InGaN (20% indium content), and GaN (0% indium content) nanoparticles on a GaN surface all show a similar size-dependent contrast reversal. This again confirms that the size-dependent ANSOM contrast reversal shown in Figure 3 is not likely to be caused by a difference in indium content of the particles between the two samples. Moreover, the simulation predicts the negative contrast even for particles with higher dielectric constant (InN and gold) than that of the substrate if the size

of the particle is sufficiently small. Indeed, Cvitkovic et al.[2] observed a similar trend in ~10 nm gold nanoparticles placed on a silicon substrate. If the particle size (hence the polarizability) is sufficiently large such that the particle dipole is stronger than the image dipole of the tip, the overall coupling is dominated by the tip−particle coupling, and this will generate positive contrast for the particle compared to the substrate. On the other hand, as we shrink down the particle size such that the particle dipole is smaller than the image dipole of the tip formed on the substrate, the overall coupling will be dominated by the tip−image dipole coupling. With the ANSOM operating in the constant-gap mode, the small particle only acts as a "spacer" that increases the tip−substrate distance, which decreases the ANSOM signal. At the same time, the decreased tip−image dipole coupling is not compensated by the weak tip−particle interaction because of the small polarizability of the particle. All of the contrast curves for different particles converge to that of the "invisible" (unit dielectric constant) particle limit (see dash−dot trace of Figure 6). The universal nature of this contrast reversal for very small particles (<10 nm) further indicates that small nano-objects placed within the tip−substrate gap preserves the cavity modes formed between the tip and the substrate, which is an important prerequisite condition for realizing nanocavity spectroscopy, as recently demonstrated by Cvitkovic et al.[2]

The contrast reversal due to the competitive coupling we have observed is most likely not limited to dielectric nano-objects. Rather, we expect that a similar contrast reversal will be observed for any small metallic, semiconducting, or polymeric nanostructures placed on high-dielectric surfaces.

Acknowledgment. We gratefully acknowledge support from the National Science Foundation, under grant NSF-DMR-0302446, as well as support for equipment from the Director, Office of Science, Office of Basic Energy Sciences, U.S. Department of Energy under contract DE-AC02-05CH11231. Z.H.K. and S.H.A. gratefully acknowledge the support from CRM-Korea Science Foundation. We thank Dr. Rainer Hillenbrand and Dr. Fritz Keilmann for valuable discussions.

References

(1) Brehm, M.; Taubner, T.; Hillenbrand, R.; Keilmann, F. *Nano Lett.* **2006**, *6*, 1307.
(2) Cvitkovic, A.; Ocelic, N.; Aizpurua, J.; Guckenberger, R.; Hillenbrand, R. *Phys. Rev. Lett.* **2006**, *97*, 060801.
(3) Frey, H. G.; Witt, S.; Felderer, K.; Guckenberger, R. *Phys. Rev. Lett.* **2004**, *93*, 200801.
(4) Hartschuh, A.; Sanchez, E. J.; Xie, X. S.; Novotny, L. *Phys. Rev. Lett.* **2003**, *90*, 095503.
(5) Ichimura, T.; Hayazawa, N.; Hashimoto, M.; Inouye, Y.; Kawata, S. *Appl. Phys. Lett.* **2004**, *84*, 1768.
(6) Kim, Z. H.; Leone, S. R. *J. Phys. Chem. B* **2006**, *110*, 19804.
(7) Kim, Z. H.; Liu, B.; Leone, S. R. *J. Phys. Chem. B* **2005**, *109*, 8503.
(8) Knoll, B.; Keilmann, F. *Nature* **1999**, *399*, 134.
(9) Kuhn, S.; Hakanson, U.; Rogobete, L.; Sandoghdar, V. *Phys. Rev. Lett.* **2006**, *97*, 017402.
(10) Novotny, L.; Stranick, S. J. *Annu. Rev. Phys. Chem.* **2006**, *57*, 303.
(11) Ocelic, N.; Huber, A.; Hillenbrand, R. *Appl. Phys. Lett.* **2006**, *89*, 101124.
(12) Taubner, T.; Hillenbrand, R.; Keilmann, F. *Appl. Phys. Lett.* **2004**, *85*, 5064.
(13) Taubner, T.; Korobkin, D.; Urzhumov, Y.; Shvets, G.; Hillenbrand, R. *Science* **2006**, *313*, 1595.
(14) Akhremitchev, B. B.; Sun, Y. J.; Stebounova, L.; Walker, G. C. *Langmuir* **2002**, *18*, 5325.
(15) Romanov, V.; Walker, C. G. *Langmuir* **2007**, *23*, 2829.
(16) Stebounova, L.; Akhremitchev, B. B.; Walker, G. C. *Rev. Sci. Instrum.* **2003**, *74*, 3670.
(17) Raschke, M. B.; Molina, L.; Elsaesser, T.; Kim, D. H.; Knoll, W.; Hinrichs, K.-O. *ChemPhysChem* **2005**, *6*, 2197.
(18) Bohn, J. L.; Nesbitt, D. J.; Gallagher, A. *J. Opt. Soc. Am. A* **2001**, *18*, 2998.
(19) Hamann, H. F.; Kuno, M.; Gallagher, A.; Nesbitt, D. J. *J. Chem. Phys.* **2001**, *114*, 8596.
(20) Hamann, H. F.; Gallagher, A.; Nesbitt, D. J. *Appl. Phys. Lett.* **1998**, *73*, 1469.
(21) Hillenbrand, R.; Keilmann, F. *Appl. Phys. B* **2001**, *73*, 239.
(22) Hillenbrand, R.; Keilmann, F.; Hanarp, P.; Sutherland, D. S. *Appl. Phys. Lett.* **2003**, *83*, 368.
(23) Hillenbrand, R.; Taubner, T.; Keilmann, F. *Nature* **2002**, *418*, 159.
(24) Novotny, L.; Hecht, B. *Principles of Nano-Optics*, 1st ed.; Cambridge University Press: Cambridge, U.K., 2006.
(25) Hillenbrand, R.; Keilmann, F. *Phys. Rev. Lett.* **2000**, *85*, 3029.
(26) Barchiesi, D. *Appl. Opt.* **2006**, *45*, 7597.
(27) Grosges, T.; Barchiesi, D. *Appl. Opt.* **2007**, *46*, 2248.
(28) Raschke, M. B.; Lienau, C. *Appl. Phys. Lett.* **2003**, *83*, 5089.
(29) Jiang, L. F.; Shen, W. Z.; Yang, H. F.; Ogawa, H.; Guo, Q. X. *Appl. Phys. A* **2004**, *78*, 89.
(30) Wolos, A.; Palczewska, M.; Zajac, M.; Gosk, J.; Kaminska, M.; Twardowski, A.; Bockowski, M.; Grzegory, I.; Porowski, S. *Phys. Rev. B* **2004**, *69*, 115210.

NL070753K